Journal of Materials Chemistry A

ROYAL SOCIETY OF CHEMISTRY

PAPER

View Article Online
View Journal | View Issue

Cite this: J. Mater. Chem. A, 2025, 13, 37427

A base-assisted one-pot cyclization and potassium association route to a very thermally stable bistetrazole salt

Parul Saini,†[a] Jatinder Singh,†[a] Richard J. Staples[b] and Jean'ne M. Shreeve*[a]

Received 21st June 2025
Accepted 24th September 2025

DOI: 10.1039/d5ta05027h

rsc.li/materials-a

Pursuing next-generation energetic materials has prompted researchers to investigate novel combinations of structural and energetic properties. In this study, we constructed a coordination-driven bisnitroimino-tetrazole scaffold, dipotassium 1,1′-methylene bis(1-nitroimino tetrazolate) (K_2MBNIT), which exhibits ultra-high thermal stability, remarkably surpassing the thermal stability of previously reported bistetrazole-based potassium salts. The synthetic route to K_2MBNIT features two key transformations: an initial tetrazole ring opening and a subsequent ring-closing reaction to form the final bistetrazole structure. In the cyclization step, K_2MBNIT is selectively obtained from the unprecedentedly formed precursor, 1,1′-methylene bis(1-azido-1-nitroiminomethylene) (4). K_2MBNIT exhibits a decomposition temperature comparable to heat-resistant energetic materials and sensitivity akin to primary explosives, presenting a unique combination of desirable properties for modern applications such as hypersonic weapons, space missions, and deep-well drilling. The straightforward synthetic methodology, methylene-assisted structural stabilization, and superior heat resistance collectively highlight K_2MBNIT as a promising candidate for a next-generation energetic material.

Introduction

Ongoing advances in energetic materials research yield efficient design strategies for high-energy-density materials (HEDMs), thereby streamlining future material innovation.[1–6] Learning from these advances, future efforts can be directed toward innovative synthesis routes and deeper insights into the structure–property correlations of HEDMs. Energetic materials have conventionally been categorized into highly sensitive yet thermally unstable primary and secondary explosives, which offer greater thermal stability but demand strong initiation stimuli. However, modern applications such as hypersonic weapons, space missions, and deep-well drilling demand materials that can withstand high temperatures and be readily initiated under controlled conditions.[7–10]

However, combining high thermal stability with high sensitivity is inherently challenging, as sensitivity often comes at the cost of stability. Materials capable of both are rare but vital, especially in systems such as missile boosters and shaped charges, where explosives must survive intense thermal stress and still detonate precisely when needed.[11] The development of such dual-function explosives enables simplified, safer initiation systems, reduces dependence on hazardous primaries, and marks a significant step forward in bridging the gap between reliability and reactivity in energetic material design.

Tetrazole-based potassium salts have recently gained attention due to their high nitrogen content and promising energetic properties. The conjugated electronic structure of the tetrazole ring facilitates regioselective substitution at the C5 position and N1 or N3 atoms, enabling structural modifications that can precisely modulate parameters such as thermal decomposition temperature, enthalpy of formation, and detonation performance. A key strategy to enhance the safety and performance of such materials lies in introducing bridging moieties between azole units. Researchers have modulated rigidity, electronic delocalization, and intermolecular interactions by carefully engineering the molecular backbone-through methylene, azido, amino, or alkyl linkers (Fig. 1A).[12–23] These modifications often lead to improved crystal packing, π–π stacking, and hydrogen bonding, all contributing to enhanced thermal resistance and detonation performance.

Recent research has increasingly focused on potassium-based primary explosives as environmentally friendly alternatives to traditional lead-based initiators due to the more benign byproducts, primarily potassium salts formed upon combustion (Fig. 1B). However, mono-tetrazole-based energetic salts which contain nitroimino groups are only moderately stable thermally, with decomposition temperatures ranging from 128 °C to 244 °C and with high sensitivity (Fig. 1C).[24–30] Bistetrazole-based potassium salts with similar nitroimino

[a]Department of Chemistry, University of Idaho, Moscow, ID 83844-2343, USA. E-mail: jshreeve@uidaho.edu

[b]Department of Chemistry, Michigan State University, East Lansing, Michigan 48824, USA

† Authors contributed equally.

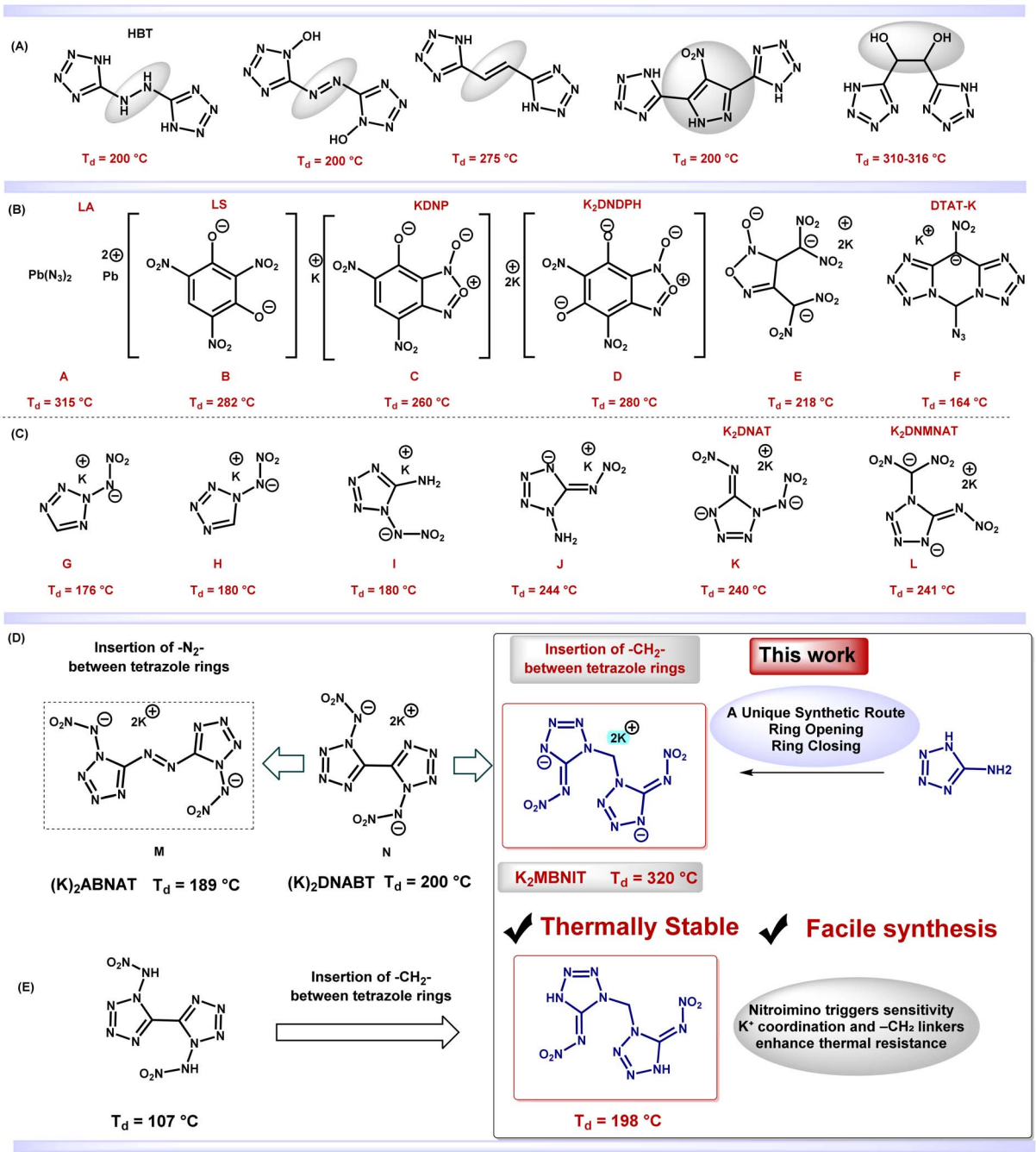

Fig. 1 (A) Bis(tetrazole)-based energetic materials with bridging moieties. (B) Primary explosives based on heavy metals, and some representative examples of green primary explosives. (C) Potassium salts based on a monotetrazole ring. (D and E) Comparison of nitro group-containing bis-tetrazole-based energetic materials and this work.

functionalities, such as **K_2DNABT**, exhibit somewhat limited thermal stability, decomposing around 200 °C. Incorporating azide-bridged linkers in bistetrazole salts, as seen in **K_2ABNAT**, further reduces their thermal robustness (Fig. 1D). While these frameworks offer good high sensitivity, their thermal stabilities remain moderate.[31,32]

To address this challenge and achieve a rare combination of high thermal stability and adequate sensitivity, we report a compound integrating a tetrazole ring for a high heat of formation, a nitroimino group to enhance sensitivity, and a methylene (–CH_2) bridge with a potassium counterion to improve stability (Fig. 1E). The potassium salt, guided by coordination chemistry principles, enables the precise assembly of the anionic framework into a stable, well-organized structure.

K_2MBNIT exhibits exceptional thermal stability, high sensitivity, and favorable predicted detonation performance based on theoretical calculations. These results broaden the structural

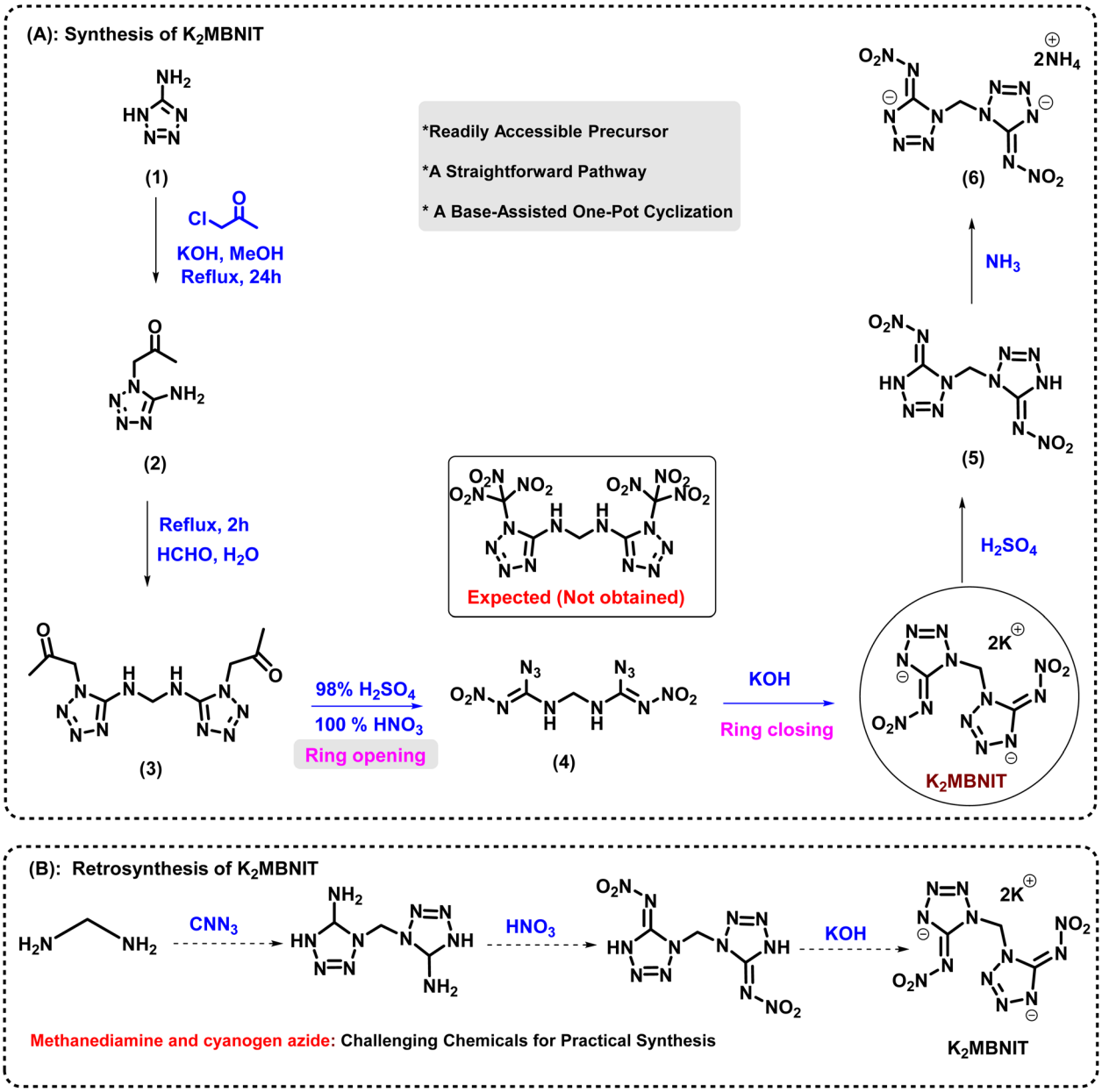

Scheme 1 (A) Synthesis of dipotassium 1,1′-methylene bis(1-nitroimino tetrazolate) (K_2MBNIT), **5** and **6**. (B) retrosynthesis of K_2MBNIT.

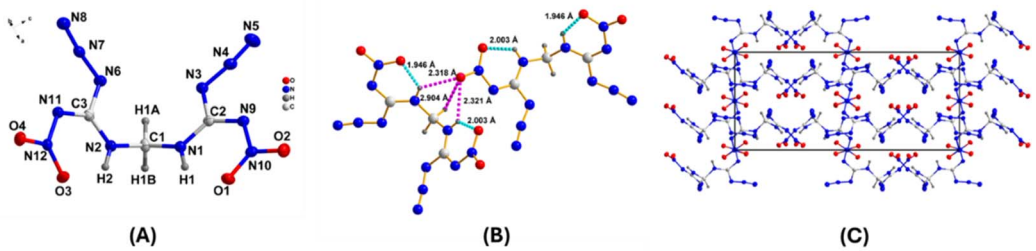

Fig. 2 (A) Drawing at 50% ellipsoids of compound **4**. (B) Representation of hydrogen bonding present in compound **4**. (C) Packing diagram of **4**.

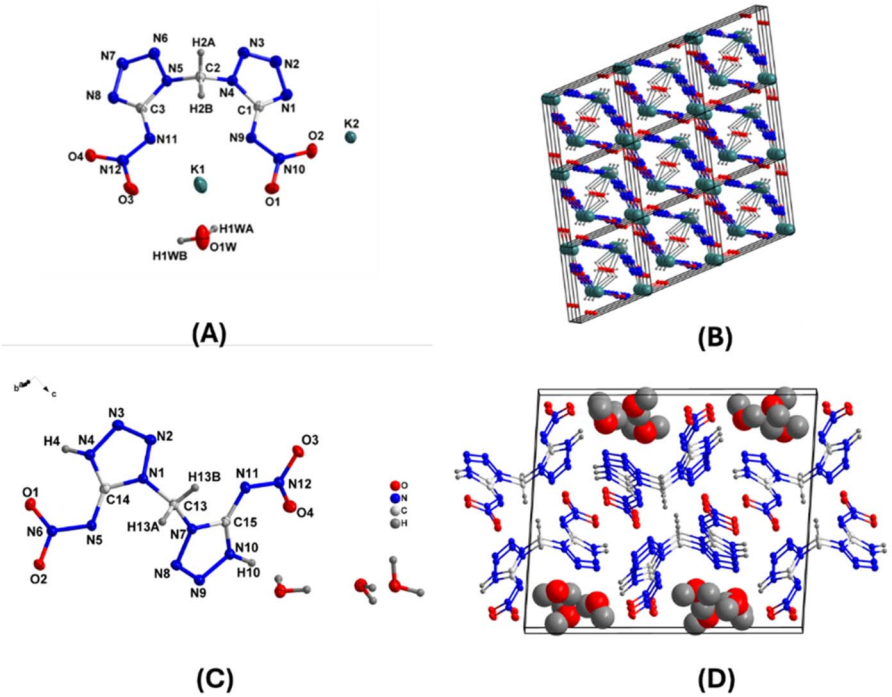

Fig. 3 (A and C) Drawing at 50% ellipsoids of compound **K_2MBNIT** H_2O and **5**·3H_2O. (B and D) Packing diagram of **K_2MBNIT** H_2O and **5**·3H_2O.

landscape of tetrazole-based energetic materials and open new avenues for developing next-generation, environmentally friendly explosives.

Results and discussion

The methylene-bridged bistetrazole salt **K_2MBNIT** synthesis is initiated using commercially available 5-aminotetrazole (**1**) as the starting material (Scheme 1A).

Initially, the synthesis of compound **2** is based on literature.[33] Subsequent treatment of compound **2** with formaldehyde in aqueous solution yields compound **3**, featuring a methylene bridge between tetrazole units. However, when compound **3** was subjected to nitration using mixed acid (HNO_3/H_2SO_4), degradation of the tetrazole ring occurs, leading to the formation of compound **4**. Compound **4** was treated with aqueous potassium hydroxide (KOH) to regenerate the tetrazole framework, successfully giving the target potassium salt **K_2MBNIT**. To access the corresponding neutral species (**5**), **K_2MBNIT** was acidified using dilute sulfuric acid under controlled conditions. Finally, the ammonium salt (**6**) was synthesized by reacting compound **5** with 40% aqueous ammonia.

During retrosynthetic analysis, it was observed that the insertion of a $-CH_2^-$ group between two tetrazole rings required methanediamine as a key precursor (Scheme 1B). However, the high cost of methanediamine compared to 5-aminotetrazole limits its practicality for large-scale applications. Although the

Table 1 Physicochemical properties of the new compounds and comparison with traditional primary explosives

Comp.	T_d[a] (°C) (onset)	$OB_{CO/CO2}$(%)	ρ[b] (g cm^{-3})	ΔH_f[c] (kJmol^{-1})	P[d] (GPa)	D_v[e] (ms^{-1})	IS[f] (J)	FS[g] (N)
4	122	−23.5/−5.8	1.74[h]	831.2	32.7	8888	2.5	<10
K_2MBNIT	320	−4.5/−18.3	2.08	336.9	31.2	8713	2	<10
K_2MBNIT.H_2O	320	−4.3/−17.4	2.00[h]	95.15	26.8	8039	3	10
5	198	−5.8/−23.5	1.69	848.6	31.6	8824	5	20
6	223	−20.9/−36.5	1.61	651.2	28.7	8562	5	20
LA[i]	315	−11/—	4.08	450.1	33.8	5920	2.5–4	1
LS[i]	282	−5.7/—	3.06	−835	—	5200	2.5–5	1.5
KDNP[j]	260	0/—	1.95	−461.7	20.01	6952	0.047	9.81
DTAT-K[k]	163.6	−19.4/—	1.88	326.4	31.7	7917	1	20
K_2DNABT[l]	200	−4.8/—	2.11	970.97	25.2	8330	5	<1

[a] Temperature (onset) of decomposition. [b] Density at 25 °C using gas pycnometer. [c] Molar enthalpy of formation, calculated using isodesmic reactions with the Gaussian 03 suite of programs (revision D.01). [d] Detonation pressure. [e] Detonation velocity (calculated using EXPLO5 version 7.01.01). [f] Sensitivity to impact (IS). [g] Sensitivity to friction (FS). [h] X-ray density calculated at room temperature (RT). [i] Ref. 37. [j] Ref. 38. [k] Ref. 39. [l] Ref. 31.

retrosynthetic route involves only three steps compared to the synthetic route, which involves four steps, it employs the highly reactive reagent cyanogen azide (CNN_3), which poses significant handling challenges compared to chloroacetone. This further restricts its feasibility for practical synthesis.[34]

Single-crystal X-ray crystallography

Suitable crystals of compound **4** were obtained by the slow evaporation of the acetonitrile solvent. Compound **4** crystallizes in the orthorhombic *Pbca* space group. In the crystal structure, the nitroimino group, azide group and CH_2 bridge lie in different planes, indicating non-coplanarity (Fig. 2A). The following hydrogen bonding interactions with a maximum D–D distance of 3.1 Å and a minimum angle of 110° are present in **4**: N1–O1: 2.584 Å, N1–O4_1: 2.923 Å, N2–O3: 2.592 Å, N2–O4_1: 2.916 Å. At 101 K.

The calculated density for compound **4** is 1.797 g cm^{-3}. As shown in Fig. 2B, inter- and intramolecular hydrogen bonding interactions between the NH group and nitro groups enhance crystal packing efficiency, thereby contributing to the good

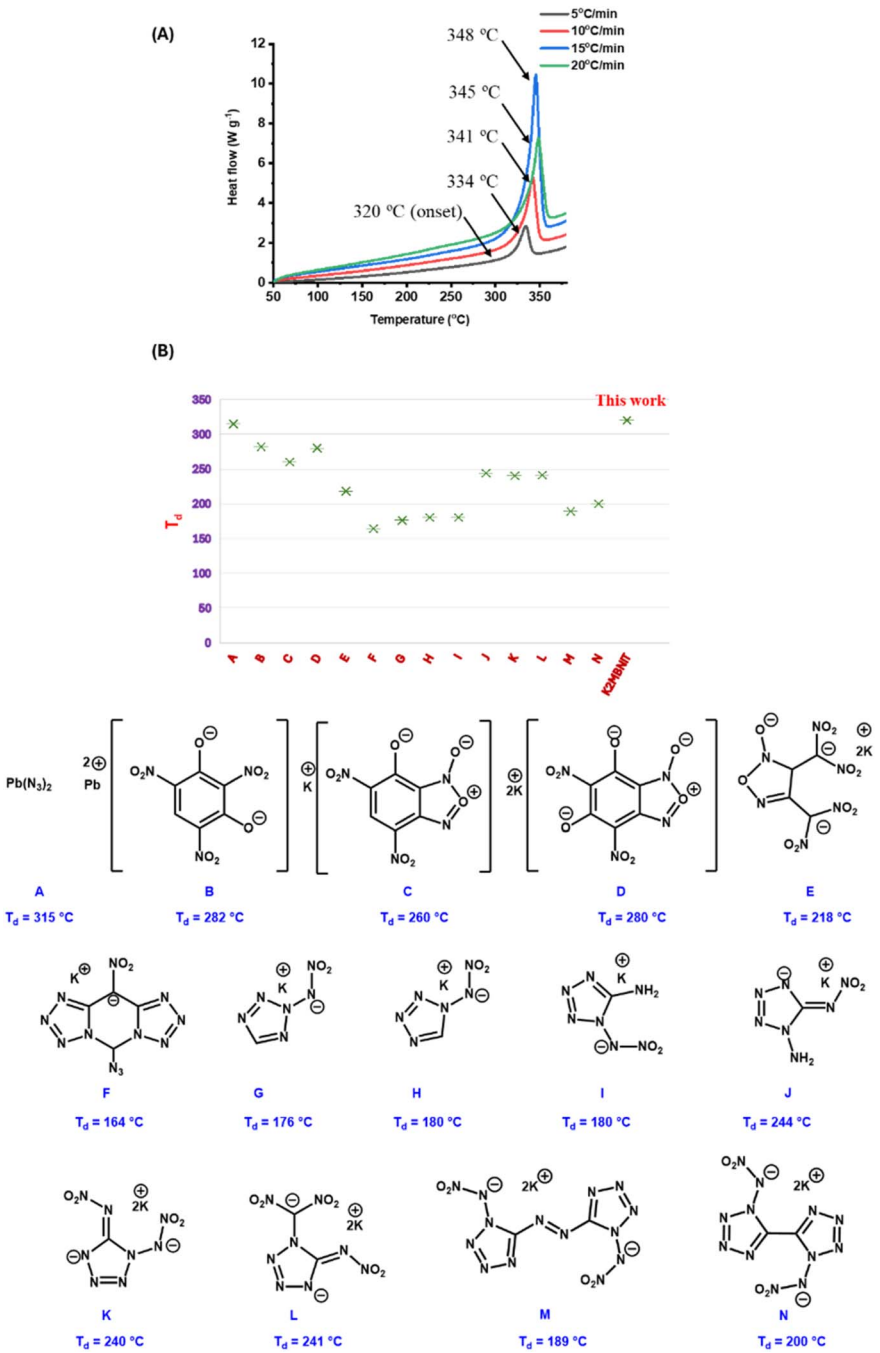

Fig. 4 (A) DSC plots of K_2MBNIT at different heating rates. (B) Comparison graph of thermal stability for A-N and K_2MBNIT.

density of **4**. The NH group of the tetrazole ring engages in an intramolecular hydrogen bond with the NO_2 group, with a bond distance of 1.964 Å, suggesting a notable stabilizing interaction within the molecular architecture. Single crystals of K_2MBNIT were obtained by dissolving the compound in water, and the resulting crystal structure revealed the presence of a water molecule within the lattice (Fig. 3A). The structure of **K_2-MBNIT**·H_2O was solved in the triclinic space group $P\bar{1}$ with a cell volume of 579.39(7) $Å^3$. The crystal of **K_2MBNIT** H_2O exhibits an excellent density of 2.026 g cm^{-3} at 213 K (Fig. 3A). As shown in Fig. 3A, the tetrazole ring, the methylene (–CH_2) group, and the nitroimino group lie in different planes, giving a non-coplanar arrangement of these structural units. Compound K_2MBNIT H_2O exhibits high molecular stability due to its rigid three-dimensional energetic metal–organic framework (3D EMOF) structure[40] (Fig. 3B).

Single crystals of **5**·3H_2O crystallize in the monoclinic space group $P2_1/c$ with a crystal density of 1.742 g cm^{-3} at 100 K (Fig. 3C). As shown in Fig. 2A, and similar to the crystal structure of compound **K_2MBNIT** H_2O, the tetrazole ring, the methylene (–CH_2) group, and nitroimino group adopt a non-coplanar arrangement (Fig. 3D).

Physicochemical and detonation properties

All compounds were analyzed in the anhydrous state, and for K_2MBNIT H_2O, the crystalline form was used. The thermal behaviors of compounds **4**, **K_2MBNIT**, **K_2MBNIT**H_2O, **5**, and **6** were analyzed using differential scanning calorimetry (DSC) at a heating rate of 5 °C min^{-1} under an N_2 atmosphere (Table 1). Among these, the dipotassium salt (**K_2MBNIT**) exhibited the highest decomposition temperature at 320 °C. The decomposition temperatures of compounds **5** and **6** are 198, and 166 °C, respectively. Based upon peak decomposition temperatures measured by differential scanning calorimetry (DSC) for compound **K_2MBNIT** at different heating rates of 5, 10, 15, and 20 °C min^{-1} (Fig. 4A), the activation energies (E_k and E_0), and linear correlation coefficients (R_k and R_0) were calculated using both the Kissinger[35] and Ozawa[36] methods and are given in Tables S5 and S6 (SI). The results show that the activation energy calculated by either method is usually very close (within ±5–10 kJ mol^{-1}) (E_k = 300.6 kJ mol^{-1}; E_0 = 295.6 kJ mol^{-1}). Depending upon the calculated numerical values of E_k, the rate constant of decomposition can be expressed as $\ln k = \ln A_k - (300.6 \times 103)/RT$.

The activation energy of **K_2MBNIT**, measured to be approximately 300 kJ mol^{-1}, indicates good thermal stability of the compound. To show the comparison of the thermal stability of A-N with **K_2MBNIT** H_2O, a scattered graph is shown in Fig. 4B. This graph shows the remarkable thermal stability of **K_2MBNIT** H_2O.

The Hirshfeld surface analyses and 2D fingerprints for **K_2MBNIT** H_2O and **5**·3H_2O were performed and are given in Fig. 5(A–F). On the edges of the Hirshfeld surface of **K_2MBNIT** H_2O many red regions (high close-contact population) were observed, mainly due to coordination bonds, *i.e.*, K/O contacts, which contribute 18.3% to the total interactions. In compound **5**·3H_2O, the red sites are due to the intermolecular hydrogen bond interactions. The total H-bond interactions, O–H/N and N–H/N, are for **K_2MBNIT** H_2O and **5**·3H_2O are 26.4% and 57.9% respectively.

The impact and friction sensitivities of all compounds were assessed using BAM standard methods, and the results are summarized in Table 1. Notably, compound **K_2MBNIT** H_2O exhibited better friction sensitivity (FS) than **LA**, **LS**, **KDNP**, and **K_2DNABT**. The experimental densities of compounds **5** and **6** were measured using a gas pycnometer at 25 °C. For compound

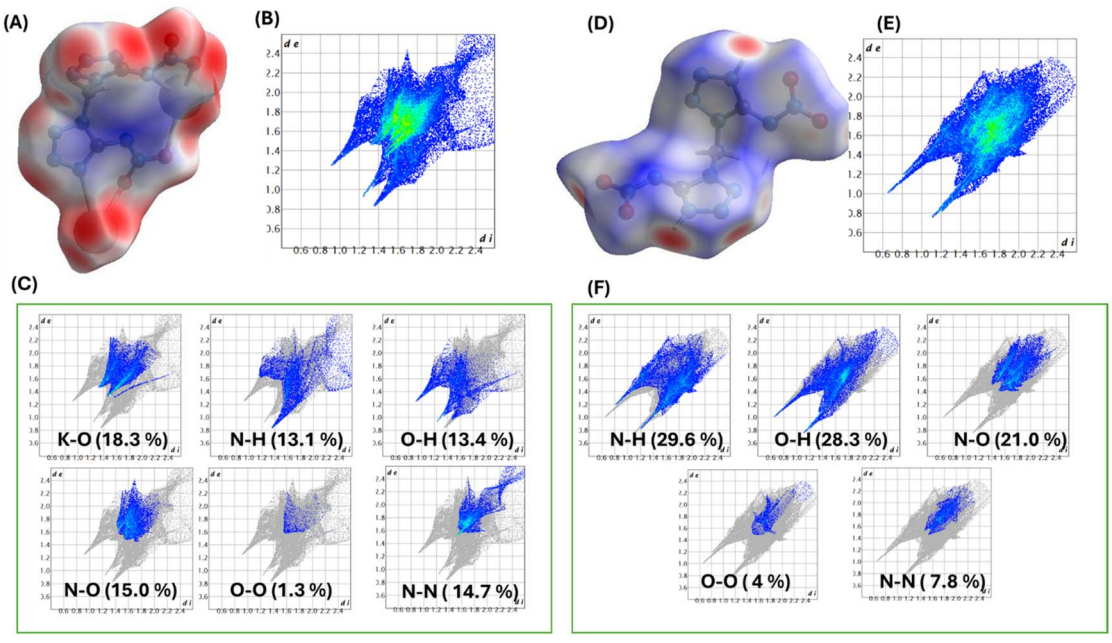

Fig. 5 (A and D) Hirshfeld surfaces for **K_2MBNIT** and **5** (B, C, E and F) 2D fingerprint plots for compound **K_2MBNIT** and **5**.

K_2MBNIT H_2O, the X-ray density was calculated at room temperature (Table 1). The densities and calculated enthalpies of formation were further utilized in the EXPLO5 (v7.01.01) software to predict the detonation properties of these compounds. The results indicated that compound **5** exhibits the highest calculated detonation velocity of 8824 m s^{-1}.

The detonation velocity of **K_2MBNIT** surpassed that of **LA**, **LS**, **DTAT-K**, and **KDNP**, suggesting enhanced explosive characteristics. The thermal stability of **K_2MBNIT** is superior to that of **LS**, **DTAT-K**, **K_2DNABT**, and **KDNP**, and is comparable to that of **LA**. Additionally, **K_2MBNIT** H_2O exhibits an oxygen balance (CO) of −4.3%, which is more favorable than those of **LA**, **LS**, and **DTAT-K**.

In conclusion, the introduction of a methylene bridge between two nitroimino-substituted tetrazole rings was found to be a highly effective structure modification for enhancing the thermal stability of bistetrazole-based energetic materials. The new potassium salt, **K_2MBNIT**, exhibits an outstanding decomposition temperature (320 °C), surpassing many traditional potassium-based and heavy metal primary explosives, such as **LS**, **KDNP**, and **K_2DNABT**. This remarkable thermal robustness is attributed to the structural stabilization conferred by the $-CH_2^-$ bridge and the coordination interactions between potassium ions and oxygen atoms, as supported by single-crystal X-ray crystallography and Hirshfeld surface analyses.

Conflicts of interest

There are no conflicts to declare.

Data availability

All data relevant to the work described here are available in the supplementary information (SI). Supplementary information: synthesis of compounds, characterization data, isodesmic reactions. See DOI: **https://doi.org/10.1039/d5ta05027h**.

CCDC 2464811–2464813 contain the supplementary crystallographic data for this paper.[41a–c]

Acknowledgements

The diffractometer (Rigaku Synergy S) for SC-XRD was purchased with support from the National Science Foundation (MRI program) under grant no. 1919565. We are grateful to the Fluorine-19 fund for support.

References

1 P. Bhatia, P. Das, A. Bijlwan and D. Kumar, *Org. Lett.*, 2024, **26**, 9781–9786.
2 T. M. Klapötke, *Chemistry of High-Energy Materials*, Walter de Gruyter & Co, KG, Berlin-New York, 2nd edn, 2012.
3 J. Cai, T. Fei, R. Li, J. Xiong, J. Zhang, P. Yin and S. Pang, *ACS Appl. Mater. Interfaces*, 2022, **14**, 52951–52959.
4 P. Bhatia, P. Das and D. Kumar, *ACS Appl. Mater. Interfaces*, 2024, **16**(47), 64846–64857.
5 J. Li, Y. Liu, W. Ma, T. Fei, C. He and S. Pang, *Nat. Commun.*, 2022, **13**, 5697.
6 C. Zhang, C. Sun, B. Hu, C. Yu and M. Lu, *Science*, 2017, **355**, 374–376.
7 T. Yan, H. Yang, C. Yang, Z. Yi, S. Zhu and G. Cheng, *J. Mater. Chem. A*, 2020, **8**, 23857–23865.
8 T. Yan, J. Ma, H. Yang and G. Cheng, *Chem. Eng. J.*, 2022, **429**, 132416.
9 G. Zhang, W. Hu, J. Ma, H. Yang and G. Cheng, *Chem. Eng. J.*, 2021, **426**, 131297.
10 H. Gao, Q. Zhang and J. M. Shreeve, *J. Mater. Chem. A*, 2020, **8**, 4193–4216.
11 C. Li, C. Deng, B. Zhao, M. Wang, M. Zhang and Z. Zhou, *Propellants, Explos., Pyrotech.*, 2020, **45**, 531–535.
12 M. Krawiec, S. R. Anderson, P. Dubé, D. D. Ford, J. S. Salan, S. Lenahan, N. Mehta and C. R. Hamilton, *Propellants Explos. Pyrotech.*, 2015, **40**, 457–459.
13 L. Zhai, X. Fan, B. Wang, F. Bi, Y. Li and Y. Zhu, *RSC Adv.*, 2015, **5**, 57833–57841.
14 X. Yu, J. Tang, C. Lei, C. Xue, G. Cheng, C. Xiao and H. Yang, *J. Mater. Chem. A*, 2024, **12**, 19513–19520.
15 X. Yu, J. Tang, C. Lei, C. Xue, H. Yang, C. Xiao and G. Cheng, *J. Mater. Chem. A*, 2024, **12**, 29638–29644.
16 J. Liu, Y. Dong, M. Li, Y. Liu, W. Huang, C. Xiao, G. Cheng and Y. Tang, *J. Org. Chem.*, 2025, **90**(11), 4054–4061.
17 B. Wang, X. Qi, W. Zhang, K. Wang, W. Lia and Q. Zhang, *J. Mater. Chem. A*, 2017, **5**, 20867–20873.
18 J. E. Zuckerman, M. C. St Myer, M. Zeller and D. G. Piercey, *ChemPlusChem*, 2025, **90**, e202400164.
19 J. Singh, R. J. Staples and J. M. Shreeve, *J. Mater. Chem. A*, 2023, **11**, 12896–12901.
20 Y. Yang, W. Zhang, S. Pang, H. Huang and C. Sun, *J. Org. Chem.*, 2024, **89**, 12790–12794.
21 F. Meng, R. Zhou, Z. Xu, P. Wang, Y. Xu and M. Lu, *J. Org. Chem.*, 2025, **90**, 3964–3973.
22 K. Hafner, T. M. Klapötke, P. C. Schmid and J. Stierstorfer, *Eur. J. Inorg. Chem.*, 2015, **2015**, 2794–2803.
23 M. Benz, T. M. Klapötke and J. Stierstorfer, *Org. Lett.*, 2022, **24**, 1747–1751.
24 Y. N. Li, B. Z. Wang, Y. J. Shu, L. J. Zhai, S. Y. Zhang, F. Q. Bi and Y. C. Li, *Chin. Chem. Lett.*, 2017, **28**, 117–120.
25 N. Szimhardt, M. H. H. Wurzenberger, P. Spieß, T. M. Klapötke and J. Stierstorfer, *Propellants Explos. Pyrotech.*, 2018, **43**, 1203–1209.
26 M. Benz, T. M. Klapötke, J. Stierstorfer and M. Voggenreiter, *ACS. Appl. Eng. Mater.*, 2023, **1**, 3–6.
27 Q. Yu, P. Yin, J. Zhang, C. He, G. H. Imler, D. A. Parrish and J. M. Shreeve, *J. Am. Chem. Soc.*, 2017, **139**, 8816–8819.
28 J. Singh, R. J. Staples and J. M. Shreeve, *Sci. Adv.*, 2023, **9**, eadk3754.
29 S. G. Zlotin, I. L. Dalinger, N. N. Makhova and V. A. Tartakovsky, *Russ. Chem. Rev.*, 2020, **89**, 1–54.
30 O. T. O'Sullivan and M. J. Zdilla, *Chem. Rev.*, 2020, **120**, 5682–5744.
31 D. Fischer, T. M. Klapötke and J. Stierstorfer, *Angew. Chem., Int. Ed.*, 2014, **53**, 8172–8175.

32 D. Fischer, T. M. Klapötke and J. Stierstorfer, *Angew. Chem., Int. Ed.*, 2015, **54**, 10299–10302.
33 P. Saini, J. Singh, R. J. Staples and J. M. Shreeve, *J. Mater. Chem. A*, 2025, **13**, 17421–17428.
34 B. Wang, X. Qi, W. Zhang, K. Wang, W. Li and Q. Zhang, *J. Mater. Chem. A*, 2017, **5**, 20867–20873.
35 H. E. Kissinger, *Anal. Chem.*, 1957, **29**, 1702–1706.
36 T. A. Ozawa, *Bull. Chem. Soc. Jpn.*, 2006, **38**, 1881–1886.
37 Q.-u.-N. Tariq, S. Manzoor, M.-u.-N. Tariq, W. L. Cao and J. G. Zhang, *Def. Technol.*, 2022, **18**, 1945–1959.
38 M. A. Ilyushin, I. V. Tselinsky and I. V. Shugalei, *Cent. Eur. J. Energ. Mater.*, 2012, **9**, 293–328.
39 K. Pandey, A. Tiwari, J. Singh, P. Bhatia, P. Das, D. Kumar and J. M. Shreeve, *Org. Lett.*, 2024, **26**, 1952–1958.
40 J. Singh, A. K. Chinnam, R. J. Staples and J. M. Shreeve, *Inorg. Chem.*, 2022, **61**, 16493–16500.
41 (*a*) CCDC 2464811: Experimental Crystal Structure Determination, 2025, DOI: **10.5517/ccdc.csd.cc2nqv19**; (*b*) CCDC 2464812: Experimental Crystal Structure Determination, 2025, DOI: **10.5517/ccdc.csd.cc2nqv2b**; (*c*) CCDC 2464813: Experimental Crystal Structure Determination, 2025, DOI: **10.5517/ccdc.csd.cc2nqv3c**.